2024 IEEE International Conference on Robotics and Automation (ICRA 2024)
May 13-17, 2024. Yokohama, Japan

A Phase-Change Emulsion Jamming Gripper for Manipulation of Micro-Scale Textured Surfaces

Alex Keller[1], Tianqi Yue[1*], Qiukai Qi[1], Andrew T. Conn[1] and Jonathan Rossiter[1]

***Abstract*— The inherent elasticity of soft materials can be used to create robotic grippers that deform and comply to a variety of irregular shapes. To date, several soft adaptive grasping strategies have been reported, however, most of them focus on adapting to the overall shape of the structure, while the adaptive grasping of small surface asperities is overlooked. In this paper, we propose a novel method to achieve adaptive grasping on surface asperities with a smart shape-memory silicone sponge. Heating above 60°C makes the sponge soft and deformable to allow it to penetrate within surface asperities via a pressure normal to the surface. Cooling down below 60°C makes the sponge "jam" to retain its deformed shape. The interlocking force between the jammed sponge and the asperities, and the increased area of contact, allows for adaptive grasping on asperities down to 0.4 mm with an adhesive force of up to 27.7 N in a 40 × 40 mm contacting area. We introduce the design, working principle, fabrication, and optimization of a robotic gripper based on this shape-memory silicone sponge. This sponge-jamming gripper shows great potential for developing next-generation robotic grippers for the manipulation of textured and discontinuous surfaces.**

I. Introduction

Adaptive grasping of irregular objects and delicate textures is a challenge for the current state-of-the-art of robotic grippers. To address this problem, granular-jamming grippers have been developed to grasp irregular-shaped objects [1]–[5]. By enclosing rigid granules within an elastic membrane and applying a vacuum, the granules jam together to increase stiffness and tightly grip extrusions on an object [6], [7]. However, the sizes of granular-jamming grippers are typically large (∼10 cm) severely limiting their conformation on surfaces with smaller irregularities (henceforth referred to as asperities) and on flat and textured surfaces [8], [9]. In addition, granular-jamming grippers usually have a relatively high weight due to the filler and air pump. In the field of adaptive grasping of small asperities, phase-changing materials have been reported to be effective, such as rubbery-glassy (RG) phase-changing materials [10]–[12] including hot adhesives [13], [14], shape-memory polymers [10], [11], [15], [16], and liquid-solid (LS) phase-changing materials like gallium [17], [18]. Pushing rubbery-state RG materials onto a surface and then transitioning them to the glassy state can make the RG material interlock with asperities. However, the rubbery-state RG materials may lack elasticity. Similarly, dropping liquid-state LS materials on the surface and then solidifying them can also generate interlocking forces. However, recovering the LS materials from the micro gaps is a challenge due to the absence of elastic return. To address these problems, we propose a sponge-jamming method for adhering to surface asperities with high adaptation, easy removal and recovery, and no need for a pneumatic pump.

The key component of our proposed sponge-jamming gripper is a shape-memory silicone sponge, which is a simple composite of silicone and paraffin wax (PW). It stores mechanical deformation in the gripping state and returns to its original shape when reheated. The PW globules are uniformly distributed within the silicone matrix and when they are in their solid phase, they increase the stiffness of the silicone matrix via a mechanism analogous to granular jamming, which we have named phase-change emulsion (PCE) jamming. Conversely, when the globules are heated above their transition temperature ($\gtrsim$60°C [19]) the PW starts to become liquid, the PCE jamming mechanism is removed, and the silicone matrix becomes soft again. In this soft state, the silicone sponge (SS) exhibits high elasticity which is able to easily penetrate deeply into microscale asperities [20]–[22]. As the globules cool down and re-

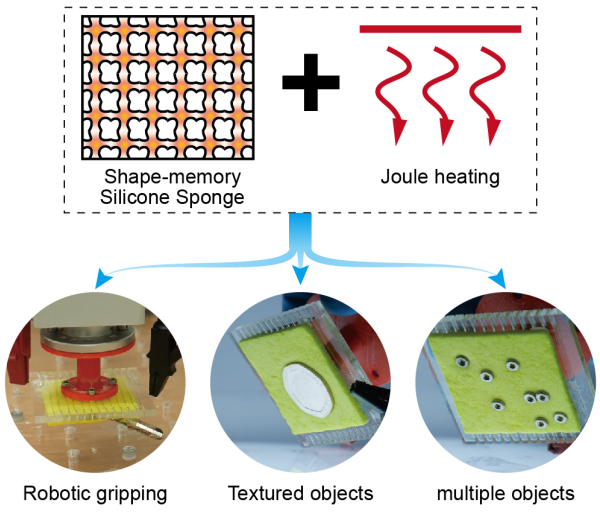

Fig. 1. The proposed shape-memory sponge-jamming gripper.

[1]Alex Keller, Tianqi Yue, Qiukai Qi, Andrew Conn and Jonathan Rossiter are with the School of Engineering Mathematics and Technology and the Bristol Robotics Laboratory at the University of Bristol, Bristol, BS8 1TW, UK. {alex.keller, tianqi.yue, qiukai.qi, a.conn, jonathan.rossiter}@bristol.ac.uk
*Corresponding author.

AK is supported by EU Horizon 2020 grant ROBOFOOD (964596) and (EPSRC) grant EP/R02961X/1. TY was funded by Chinese Scholarship Council through award 201906120027 and (EPSRC) grant EP/R02961X/1. JR was supported through EPSRC research grants EP/V062158/1, EP/T020792/1, EP/V026518/1, EP/S026096/1 and EP/R02961X/1, and by the Royal Academy of Engineering as a Chair in Emerging Technologies. AC was supported by EPSRC EP/R02961X/1, EP/T020792/1 and EP/W006235/1.

solidify, the PCE jamming mechanism is reintroduced into the matrix, making it stiff again and stabilising the contact and grip of these small asperities. Grasped objects can be released from the silicone-wax gripper by once again heating the PW globules past their transition temperature, converting the PW back to its liquid phase, whereupon the silicone sponge becomes soft again. We believe this work contributes to the state of the art of robotic grippers via the introduction of phase-change jamming grippers.

II. Principle, Design and Fabrication

A. Design of the SSG

The design of the shape-memory sponge gripper (SSG) is outlined in Fig.2B. As shown in Fig.2B the base of the SSG is the SS, which is glued to a PMMA sheet with a nichrome wire wound around the PMMA sheet. Attached to the top of the PMMA sheet is a plastic holder which allows the SSG to be attached to a robotic arm. To operate, two ends of the nichrome wire are connected to an external power supply which applies a joule-heating current. Joule heating of the nichrome wires heats up the PW, and the cooling of the SS is achieved by allowing the heat to dissipate into the surrounding air. A green/yellow thermochromic pigment (SFXC, SFXCFFP) was used to help illustrate the SS transition from a cool to a hot state for the demonstration videos of the SSG gripping real-world objects.

B. Working Principle of the SSG

The working principle of the SSG is shown in Fig.2C, Fig.5 and supplementary video. When the SSG is about to grip a textured surface, current is applied to the nichrome wire for a specific duration to heat the sponge above 60°C, the melting point of the PW. After which, the sponge becomes soft (Fig.2C i). Next, a robotic arm pushes the SSG against the textured surface and maintains a preload force, causing the sponge to penetrate into the gaps of the asperities as a result of its shape conformation ability (Fig.2C ii). After conformation, the current is removed, allowing the sponge to cool down. Once the whole sponge temperature is below the melting point of the PW, the PW globules are solidified and the whole sponge is "jammed" (Fig.2C iii). The jammed sponge generates large enough contact surface area and sufficient interlocking force to the surface asperities and the robotic arm can easily pick up and manipulate the textured object (Fig.2C iv). Finally, the object can be released via re-heating the sponge, which liquefies the PW to globules again and the silicone base recovers to its original shape (Fig.2C v and supplementary video).

C. Fabrication

The PMMA sheet (thickness 3 mm) was made by laser cutting. The nichrome wire (Uxcell, Nichrome 80) has a diameter of 0.1 mm and a resistance of 138.8 Ω/m. The holder of the gripper is 3D printed with PLA (Anycubic i3 Mega S). The shape-memory silicone-PW sponge was constructed using silicone rubber (Smooth-on, Dragon Skin 10), PW (Sigma-Aldrich, CAS-No:8002-74-2) and sodium chloride (Sainsbury, SAXA). First 2.6667 grams of PW was melted on a hot plate at 90°C. Then 2 grams of silicone rubber part A was heated on a hot plate at 60°C. Whilst still hot, silicone rubber part A and PW were mechanically mixed for 5 minutes in a glass beaker. Once a homogeneous dispersion of part A and PW was achieved, 2 grams of silicone rubber part B (curing agent) was added and mechanically mixed

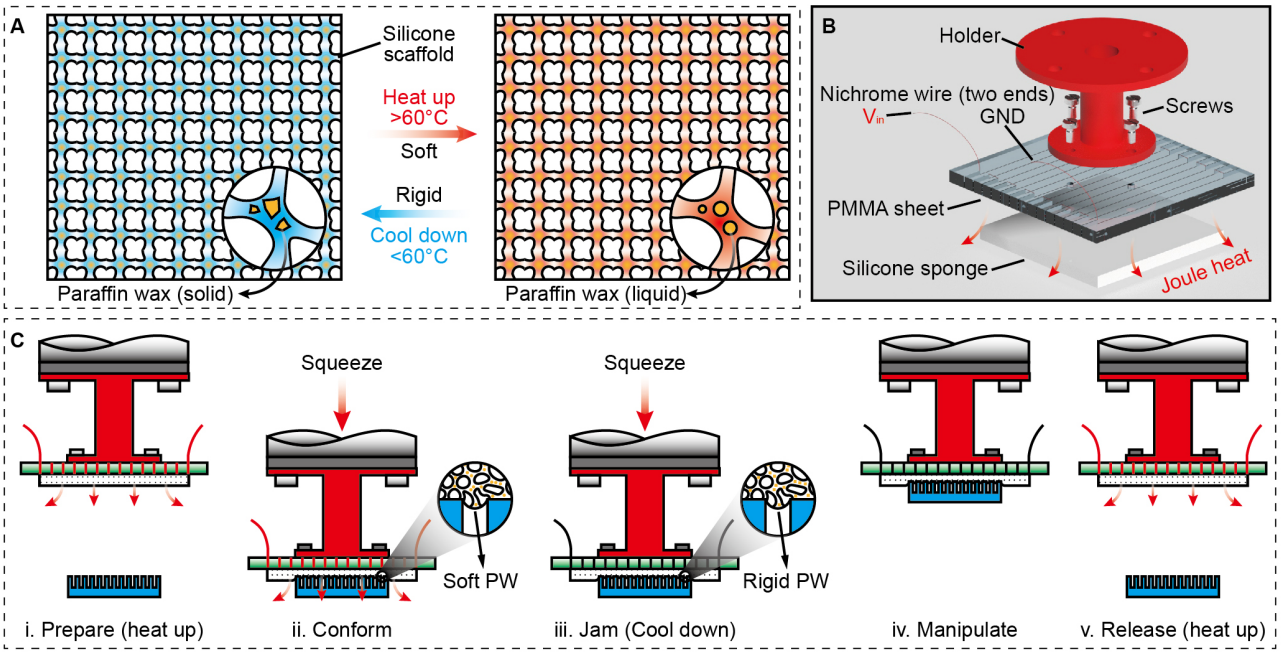

Fig. 2. The principle of the shape-memory sponge and the proposed gripper. (A) the reversible transition between rigid and soft states of the SS via the melting and solidification of the PW globules within the silicone matrix. (B) The design of the SSG. (C) The working principle of the SSG.

for 5 minutes to give a final ratio of PW to silicone rubber of 40% w/w. To this mixture, different amounts of sodium chloride powder were added and mechanically mixed for 5 minutes. Finally, the homogenous mixture of silicone rubber, PW and sodium chloride was cast into moulds and left at room temperature to cure for 4 hours. Once cured, samples were left in water overnight to promote the dissolution of the salt crystals. Finally the samples were gently massaged in hot water (80°C) for 1 hour to remove any remaining sodium chloride solid.

III. Simulations and Optimisation

A. Optimisation of the SSG

The optimisation of the SSG involves four variables: 1) the current passing through the nichrome wire, I_{wire}, 2) the number of folds of the nichrome wire in the sponge region, N_{wire}, 3) the thickness of the silicone sponge, t_{sponge}, and 4) the porosity of the silicone sponge, ϕ_{sponge}, which is the volume ratio of air chambers to the total sponge: Eq. (1).

TABLE I

Chemicals used in fabricating the sponge.

Name	ρ (g/cm^3)	k (W/m·K)	C (J/kg·K)
PW	0.9	0.25	2100
Silicone	1.07	0.2	1100
Air	1.29 $\times 10^{-3}$	0.025	700
NaCl	2.16	N/A	N/A

We first determine the porosity of the silicone sponge ϕ_{sponge}. Since the silicone sponge has an open-cell spongy structure, its porosity determines the conformation ability to surface asperities and the total thermal conductivity of the sponge. It was found that a porosity above 0.7 makes the sponge structure too weak and easy to collapse, while a porosity below 0.5 cause solid crystals of sodium chloride to remain trapped in the sponge. Therefore, five silicone sponge samples with increasing porosity, 0.5, 0.55, 0.6, 0.65, 0.7, were fabricated. Given the properties (density ρ, thermal conductivity k and heat capacity C) of PW, silicone rubber and air, shown in Tab.I, the mass ratio μ has the following relation with ϕ_{sponge}:

$$\phi_{\text{sponge}} = \frac{V_{\text{void}}}{V_{\text{total}}} = \frac{0.77\mu}{0.77\mu + 1.68}. \tag{1}$$

Therefore, the corresponding mass ratios μ used in the fabrication are shown in Tab.II.

TABLE II

Mass ratio of NaCl and wax-silicone mixture.

ϕ_{sponge}	0.5	0.55	0.6	0.65	0.7
μ	2.1818	2.6667	3.2727	4.0519	5.0909

The influence of ϕ_{sponge} on the conformation ability cannot be readily predicted. Therefore, we carried out a simple squeezing test as shown in Fig.3B. Applying the same normal preload on the sponges with the same dimensions (10×20×3 mm), the depth of the deformed sponge penetrating into the asperities of a sample surface was recorded and normalised by compressing the SS onto a grooved surface with a preload force – *Normalised adaptation = Penetration depth / Original thickness*. Results indicate that $\phi_{\text{sponge}} = 0.6$ leads to the highest texture conformation. However, to allow for effective joule heating transfer through the sponge, the total thermal conductivity must be considered, which is influenced by ϕ_{sponge}. The SS has an open-cell porous structure, indicating that it is a composite of a solid part (the mixture of the PW and the silicone rubber) and a fluid part (air). The thermal conductivity of the solid part can be estimated as:

$$k_{\text{solid}} = 0.6k_{\text{silicone}} + 0.4k_{\text{wax}} = 0.22 \text{ W/m·K}, \tag{2}$$

where 0.6 and 0.4 are the mass proportion of the silicone and wax in the mixture. The total effective thermal conductivity of the sponge k_{e} can be estimated using the effective thermal conductivity (ETC) theory [23]:

$$(1-\phi_{\text{sponge}})\frac{k_{\text{solid}} - k_{\text{e}}}{k_{\text{solid}} + 2k_{\text{e}}} + \phi_{\text{sponge}}\frac{k_{\text{air}} - k_{\text{e}}}{k_{\text{air}} + 2k_{\text{e}}} = 0. \tag{3}$$

Consequently, higher ϕ_{sponge} leads to lower k_{e} (since $k_{\text{air}} \ll k_{\text{solid}}$) which is not optimal for joule heat transferring to the outer surface of the sponge. To balance the mechanical conformation ability and thermal conductivity of the sponge, we resolved to use $\phi_{\text{sponge}} = 0.55$ for the subsequent development and characterisation of the SSG.

B. Simulations

To determine the current required to be applied to the nichrome wire I_{wire} and the thickness of the sponge t_{sponge}, we implemented finite element modelling simulations in Comsol Multiphysics. The Comsol model is an assembly with a straight nichrome wire covered by a porous silicone sponge. Basic settings in Comsol are shown in Tab.III.

TABLE III

Basic settings in Comsol.

Term	**Specification**
Study	Stationary
Material properties	As calculated above
Mesh size	Extra fine by default

A parametric sweep with combinations of $I_{\text{sponge}} = 0.1, 0.2, 0.3, 0.4, 0.5$ A and $t_{\text{sponge}} = 1, 2, 3, 4, 5$ mm was conducted. Once the computation was completed, we derived the maximum temperature (close to the wire) and the minimum temperature (on the boundary with the air environment) generated in the sponge. To obtain shape-memory functionality and ensure safety, the temperature of the sponge should be controlled to be in the following range:

$$\begin{aligned} T_{\text{min}} &> T_{\text{melt\_wax}} \approx 60^{\circ}\text{C}, \\ T_{\text{max}} &< T_{\text{flash\_wax}} = 200^{\circ}\text{C}, \end{aligned} \tag{4}$$

where T_{min} and T_{max} are the minimum and maximum temperature generated in the bulk of the sponge, $T_{\text{melt\_wax}}$ and $T_{\text{flash\_wax}}$ are the melting point and flash point of the PW.

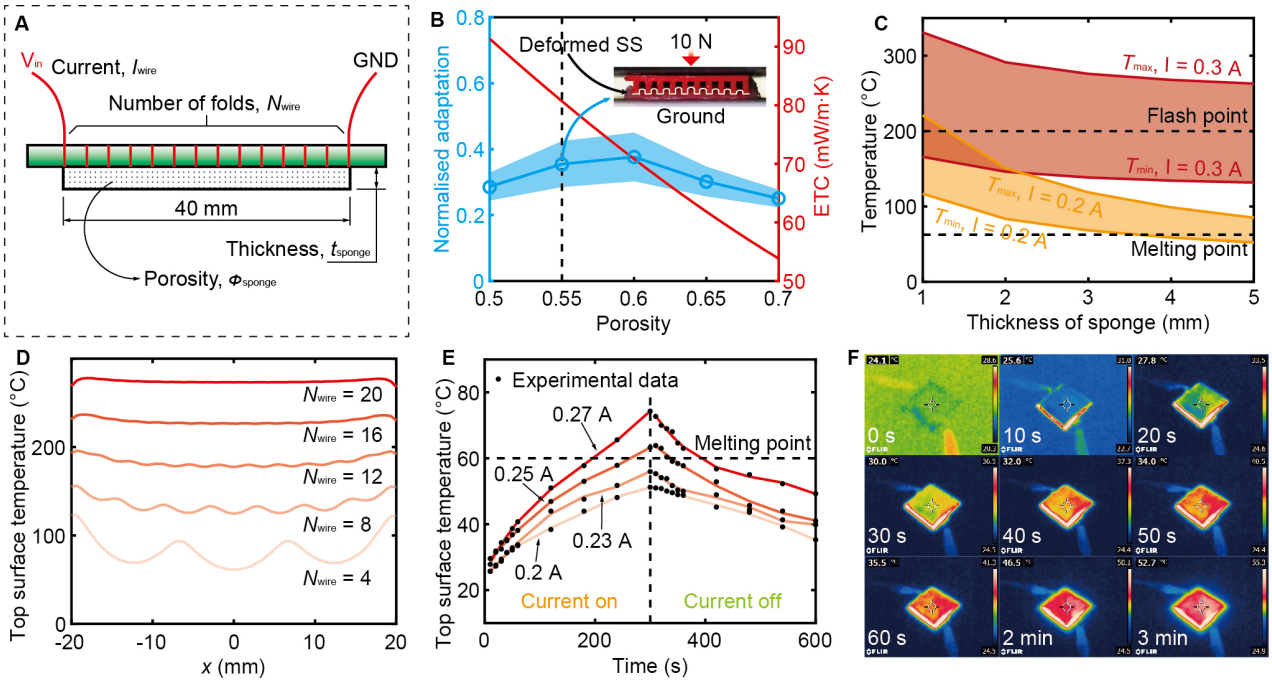

Fig. 3. The optimisation of the SSG. (A) The four parameters defining the gripper structure. (B) The determination of the optimised sponge porosity ϕ_{sponge}. (C) The simulation results of the parametric sweep between thickness t_{sponge} and current I_{wire}. (D) The simulated top surface temperature distribution on x axis across the sponge with different numbers of nichrome windings N_{wire}. (E) The measured top surface temperature of the optimised sponge. (F) Thermal camera photos of the sponge during joule heating.

The parametric sweep results are shown in Fig.3C. Only $I_{\text{wire}} = 0.2$ A and 0.3 A show compatibility with Eqn.4 and the defined operating range of $T_{\text{melt\_wax}} \sim T_{\text{flash\_wax}}$ (thus results of 0.1, 0.4 and 0.5 A are not shown). Therefore, the current applied in the wire should be within the range of 0.2∼0.3 A. In addition, Fig.3C indicates that 3 mm is the appropriate thickness for reaching the goal temperature. Based on our experiences,<3 mm is too thin to generate enough deformation on surface asperities.

To determine the number of folds of the nichrome wire N_{wire} that was weaved in parallel between the PMMA and the SS, we derive the temperature distribution on the boundary with air based on the former simulation results. When $I_{\text{wire}} = 0.2$ A is applied, this temperature distribution is shown in Fig.3D. To make the temperature distribution uniform, $N_{\text{wire}} = 16$ is selected. N_{wire}>16 will make the resistance of the nichrome wire too high for practicality.

C. Joule-heating experiments

We fabricated the optimised gripper to evaluate the joule heating and heat transfer. According to the simulation result, $I_{\text{wire}} = 0.2, 0.23, 0.25, 0.27$ A were applied, where the larger current leads to the higher heating rate. The sponge was heated up (current on) for 5 minutes and then cooled down (current off) for 5 minutes. An IR thermometer (FLUKE, 62 MAX) was used to detect the boundary temperature regularly. Results are shown in Fig.3E, which indicates that $I_{\text{wire}} = 0.27$ A is most effective for heating the boundary above $T_{\text{melt\_wax}}$ within 4 minutes. Therefore, $I_{\text{wire}} = 0.27$ A is used for the following experiments. We did not observe any flash ignition during our experiments. A thermal camera (FLIR, E4) was used to record the surface temperature increase during joule heating, as shown in Fig.3F.

IV. Experiments

The capacity for the SSG to grip a variety of different textured surfaces under different parameters was evaluated and the results are presented in Fig.4. The experimental setup contains a vertically placed linear stage, a load cell (DYLY-106) fixed on the slider of the linear stage, and the SSG gripper fixed on the ground with the sponge facing upwards (as Fig.4F shows). A current of 0.27 A was applied through the nichrome wires for 4 minutes to heat the sponge. Next, a textured sample (3D-printed with PLA, Anycubic i3 Mega S) was placed onto the SSG with various vertical (normal) preloads. After the preload was applied, the power supply to the nichrome heating wire was turned off to let the sponge cool down for 10 minutes to generate the interlocking force. Once the SSG had cooled down, the mass was removed and the textured sample was manually connected to the slider of the linear stage. Finally, the slider was moved upward at a rate of 3 mm/s for 5 mm, during which the slider generate a pulling force to detach the textured sample from the SSG. The adhesive force-displacement data was recorded, with examples (1 N and 4 N preload cases) displayed in Fig.4A. The maximum adhesive force at the moment of detachment is selected as the most important property of the SSG, which reflects the adhesive strength.

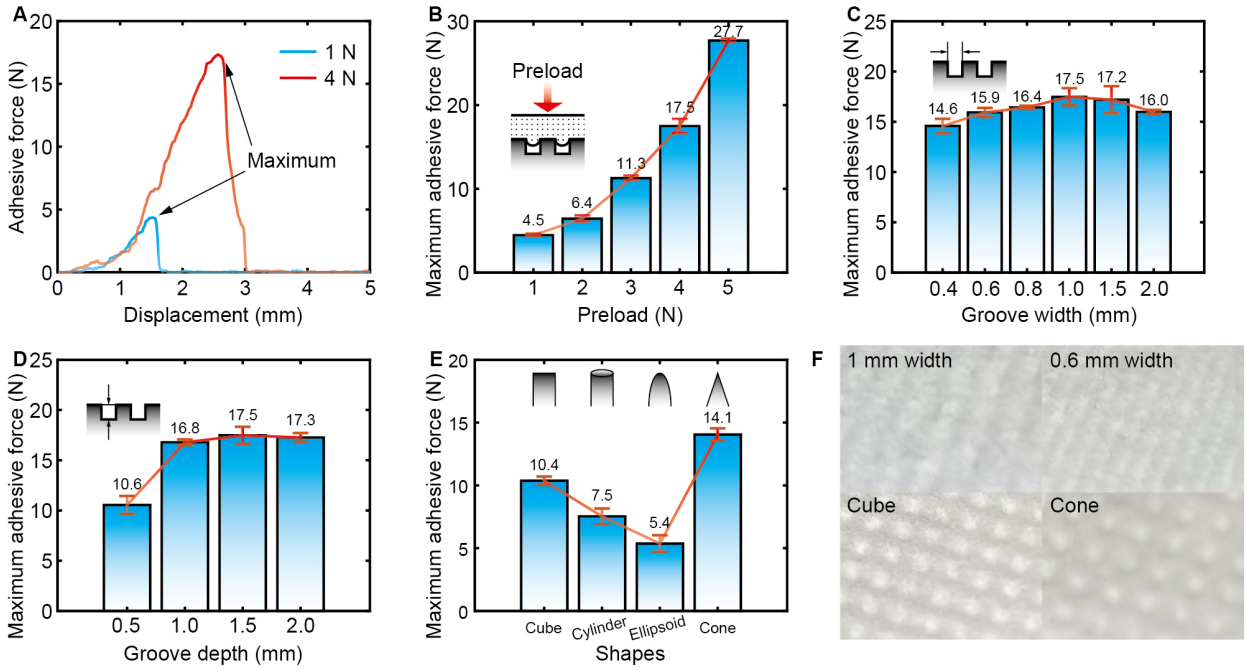

Fig. 4. The measured adhesive force of the SSG. (A) The adhesive force and corresponding displacement of the load cell from the SSG for different preload forces. (B) The relationship between the maximum adhesive force and preload force of the textured surfaces (1 mm width×1.5 mm depth) onto the SSG. (C) The maximum adhesive force vs. texture width (1.5 mm depth) with a 4 N preload force. (D) The maximum adhesive force vs. texture depth (1 mm width) with a 4 N preload force. (E) The maximum adhesive force to different shaped textures with a 4 N preload force. (F) The residual shape-memory effect of the SSG after detachment from different textured surfaces.

A. Adhesive force with different preload

We assessed the adhesive strength of the SSG under different conditions according to the measured maximum adhesive force. The standard textured sample was a 3D printed surface with an array of lines with a 1 mm opening width and 1.5 mm opening depth. To assess the effect of preload on adhesive strength, a set of 1, 2, 3, 4, and 5 N preloads were applied on the standard textured surface. The results of these tests are shown in Fig.4B. It can be seen that the preload force has a dramatic effect on the grip strength, with the preload of 1 N and 5 N resulting in a maximum adhesive force of 4.5 ± 0.5 N and 27.7 ± 0.5 N, respectively. This can be explained by the higher preload causing the sponge to penetrate more into the groove and therefore more interlocking force can be generated.

B. Adhesive force on different texture dimensions

To determine the adhesive strength of the SSG on different textured dimensions a set of 3D printed surfaces textured with an array of lines with varying separations: 0.4, 0.6, 0.8, 1.0, 1.5, and 2.0 mm, and the depth kept at 1.5 mm. A preload force of 4 N was applied to all the samples. The results are displayed in Fig.4C. It was found that the SSG was able to generate significant adhesive force to sub-millimetre textures, with the adhesive force for a 0.4 mm opening equal to 14.6 ± 1.6 N. This is a sufficiently strong adhesive force for a practical, reusable, non-residue gripper that can generate adaptive adhesion on these sub-millimetre asperities. Moreover, the gripping strength increased up to 17.5 ± 2.1 N for an opening of 1 mm width. However, the adhesive strength decreases once the opening exceeded 1 mm, reducing to 16.0 ± 0.5 N for a 2 mm width opening. We propose that the observed reduction of adhesive force for the largest and smallest openings is caused by the loss of interlocking force when the opening is too wide (i.e., contacting area reduces) or is too narrow (i.e., the sponge cell cannot penetrate into the small grooves).

We next prepared a new set of grooved samples with opening depths of 0.5, 1, 1.5, and 2 mm to assess the effect that the depth of the asperities had on the adhesive strength. All the opening widths of these samples were kept at 1 mm with an applied preload of 4 N. The results are displayed in Fig.4D. As illustrated in Fig.4D the maximum adhesive force increased from 10.6 ± 2.0 N to 17.5 ± 2.1 N when the opening depth changes from 0.5 mm to 1 mm. However, this trend of increasing adhesive force for increasing depth plateaued once the depth reached a value of 1 mm. This can be explained by the observation that the maximum penetration of the sponge under 4 N preload is approximately 1 mm and therefore no more interlocking force can be generated even when the opening depth increases.

C. Adhesive force on different texture shapes

We tested the adhesion performance of the SSG on different shapes of the asperities. Four samples with arrays of small cubes, cylinders, ellipsoids and cones were prepared. The spacing of these asperities is 1 mm and the height is

1.5 mm. 4 N preload was applied. The results are shown in Fig.4E and Fig.4F. It was observed that the SSG can generate adhesion on each of the surfaces. Fig.4E demonstrates that the SSG was less efficient at gripping rounded edges, with the cylinder and ellipsoid displaying an adhesive force of 7.5 ± 1.4 N and 5.4 ± 1.6 N, respectively. The grip strength for the cube and cone were significantly larger at 10.4 ± 0.7 N and 14.1 ± 1.1 N, respectively. This indicates that the SSG is also able to efficiently grip spiked surfaces.

D. Gripping real-world objects and robotic applications

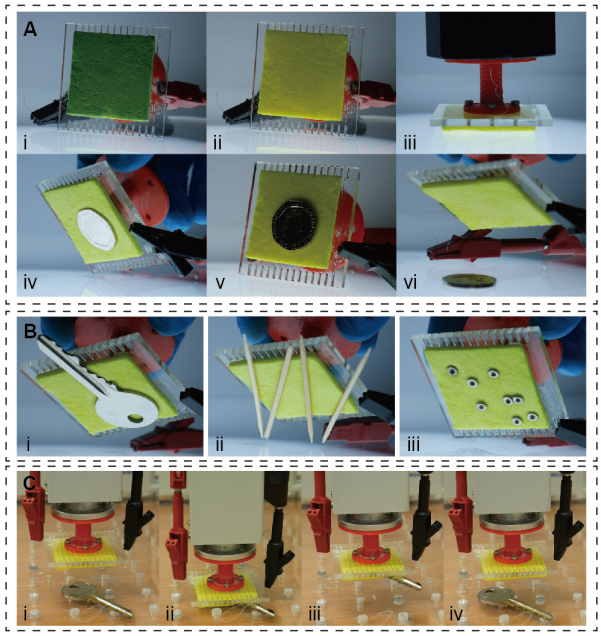

Fig. 5. Gripping real-world objects with the SSG. (A) 6 key moments during the gripping of a coin. (B) The gripping of a key, multiple toothpicks and micro nuts. (C) The automated gripping of the SSG on a robotic arm.

The ability of the SSG to grip real-world objects was explored to assess how this new gripping mechanism would translate to practical textures. The SSG was combined with a colour-changing pigment which changes from a green to yellow colour once it exceeds 31°C. The results are displayed in Fig.5, Fig.6 and the supplementary video.

Fig.5 and the supplementary video demonstrate the gripping of a variety of everyday objects with small textures and irregular shapes with SSG. In this case, we use 5 N preload since it leads to higher adhesive force according to Fig.4B. Fig.5A shows the manipulation of a coin and outlines the gripping procedure that was used; first the rigid state (i) is converted to its soft state (ii) via joule heating, then the SSG is compressed onto an object with a preload of 5 N and left to cool down for 5 minutes (iii). Once the adhesion is established the object can be lifted (iv) and manoeuvred (v). Joule heating release of the object (vi). Fig.5B illustrates the versatility of the SSG via the manipulation of a variety of irregular objects; (i) a key, (ii) several wooden toothpicks, and (iii) multiple steel nuts. Lastly, the SSG was attached to a robotic arm (Dobot MG400) to illustrate the potential of this novel type of gripper to augment robotic devices with the ability grip and manipulate textures and objects. Fig.5C demonstrates the lifting and detachment of a house key with a robotic arm simply via joule heating.

Finally, the sponge-jamming-induced shape memory of the SSG is illustrated in Fig.6. The SSG was heated and placed over a house key. Once it had conformed to the shape of the key, the current was shut off and the SS cooled down, locking in the shape of the key. The key was removed from the SSG once the shape memory was established. As can be seen, the SSG has an impressive capacity to "remember" in great detail the shape and pattern of complex textured objects. Furthermore, the detachment/recovery mechanism of the SSG is demonstrated in Fig.6 and the supplementary video via the re-application of current to the nichrome wire. This process can be repeated many times using this cheap, simple, conformable silicone-PW composite.

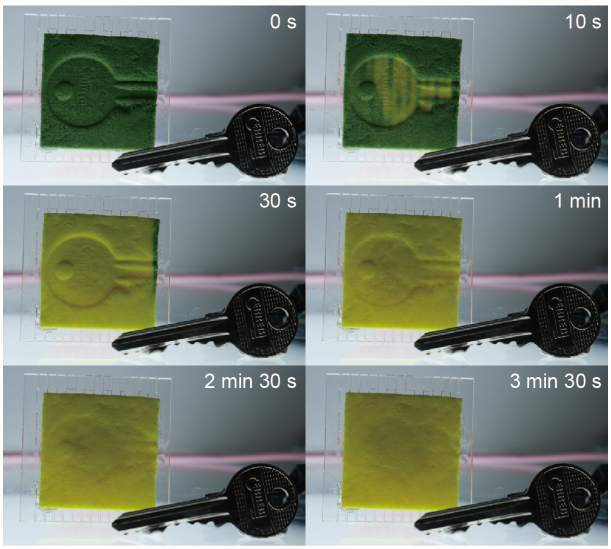

Fig. 6. The memorising and recovery (erasure) of the indentation of a key in the shape-memory silicone sponge.

V. Conclusions

Gripping textured surfaces is still a significant challenge for robotic grippers. In this paper, we proposed a shape-memory sponge-jamming gripper (SSG) to address this problem. The SSG achieved adaptive gripping on textured surfaces on the scale of < 1 mm and served as a robotic arm end effector for picking up real-world objects. The adaptive gripping on surface asperities originates from the unique phase-change emulsion jamming mechanism of this smart material which has advantages over the current state-of-the-art granular jamming grippers by lacking the need for a pneumatic pump and being able to grasp small and complex textures. This actuation was done many times during the characterisation with no visible degradation. Future development of the SSG will combine the adaptation on a macro scale with the proposed microscale gripping to broaden the application scenarios in robotics, industry and healthcare.

REFERENCES

[1] J. Shintake, V. Cacucciolo, D. Floreano, and H. Shea, "Soft robotic grippers," *Advanced materials*, vol. 30, no. 29, p. 1707035, 2018.

[2] J. Hernandez, M. S. H. Sunny, J. Sanjuan, I. Rulik, M. I. I. Zarif, S. I. Ahamed, H. U. Ahmed, and M. H. Rahman, "Current designs of robotic arm grippers: a comprehensive systematic review," *Robotics*, vol. 12, no. 1, p. 5, 2023.

[3] K. Tai, A.-R. El-Sayed, M. Shahriari, M. Biglarbegian, and S. Mahmud, "State of the art robotic grippers and applications," *Robotics*, vol. 5, no. 2, p. 11, 2016.

[4] L. Birglen and T. Schlicht, "A statistical review of industrial robotic grippers," *Robotics and Computer-Integrated Manufacturing*, vol. 49, pp. 88–97, 2018.

[5] Q. Qi, C. Xiang, V. A. Ho, and J. Rossiter, "A sea-anemone-inspired, multifunctional, bistable gripper," *Soft Robotics*, vol. 9, no. 6, pp. 1040–1051, 2022.

[6] J. R. Amend, E. Brown, N. Rodenberg, H. M. Jaeger, and H. Lipson, "A positive pressure universal gripper based on the jamming of granular material," *IEEE transactions on robotics*, vol. 28, no. 2, pp. 341–350, 2012.

[7] E. Brown, N. Rodenberg, J. Amend, A. Mozeika, E. Steltz, M. R. Zakin, H. Lipson, and H. M. Jaeger, "Universal robotic gripper based on the jamming of granular material," *Proceedings of the National Academy of Sciences*, vol. 107, no. 44, pp. 18 809–18 814, 2010.

[8] J. Amend, N. Cheng, S. Fakhouri, and B. Culley, "Soft robotics commercialization: Jamming grippers from research to product," *Soft robotics*, vol. 3, no. 4, pp. 213–222, 2016.

[9] J. M. Gómez-Paccapelo, A. A. Santarossa, H. D. Bustos, and L. A. Pugnaloni, "Effect of the granular material on the maximum holding force of a granular gripper," *Granular Matter*, vol. 23, pp. 1–6, 2021.

[10] C. Linghu, S. Zhang, C. Wang, K. Yu, C. Li, Y. Zeng, H. Zhu, X. Jin, Z. You, and J. Song, "Universal smp gripper with massive and selective capabilities for multiscaled, arbitrarily shaped objects," *Science Advances*, vol. 6, no. 7, p. eaay5120, 2020.

[11] C. Linghu, Y. Liu, Y. Y. Tan, J. H. M. Sing, Y. Tang, A. Zhou, X. Wang, D. Li, H. Gao, and K. J. Hsia, "Overcoming the adhesion paradox and switchability conflict on rough surfaces with shape-memory polymers," *Proceedings of the National Academy of Sciences*, vol. 120, no. 13, p. e2221049120, 2023.

[12] M. Pushpakath and M. H. Ang Jr, "Design of a liquid jamming gripper," *Designs*, vol. 7, no. 2, p. 44, 2023.

[13] L. Wang, L. Graber, and F. Iida, "Large-payload climbing in complex vertical environments using thermoplastic adhesive bonds," *IEEE Transactions on robotics*, vol. 29, no. 4, pp. 863–874, 2013.

[14] L. Wang and F. Iida, "Physical connection and disconnection control based on hot melt adhesives," *IEEE/ASME Transactions on mechatronics*, vol. 18, no. 4, pp. 1397–1409, 2012.

[15] C. Son, S. Jeong, S. Lee, P. M. Ferreira, and S. Kim, "Tunable adhesion of shape memory polymer dry adhesive soft robotic gripper via stiffness control," *Robotics*, vol. 12, no. 2, p. 59, 2023.

[16] Q. Qi, A. Keller, L. Tan, Y. Kumaresan, and J. Rossiter, "Edible, optically modulating, shape memory oleogel composites for sustainable soft robotics," *Materials & Design*, vol. 235, p. 112339, 2023.

[17] Z. Ye, G. Z. Lum, S. Song, S. Rich, and M. Sitti, "Phase change of gallium enables highly reversible and switchable adhesion," *Advanced Materials*, vol. 28, no. 25, pp. 5088–5092, 2016.

[18] H. Wang, S. Chen, H. Li, X. Chen, J. Cheng, Y. Shao, C. Zhang, J. Zhang, L. Fan, H. Chang, *et al.*, "A liquid gripper based on phase transitional metallic ferrofluid," *Advanced Functional Materials*, vol. 31, no. 32, p. 2100274, 2021.

[19] Sigma, "Paraffin wax sds, 76242, united kingdom," https://www.sigmaaldrich.com/GB/en/sds/aldrich/76242 Accessed September 2, 2023.

[20] L. Li, T. Hu, Y. Yang, and J. Zhang, "Strong, compressible, bendable and stretchable silicone sponges by solvent-controlled hydrolysis and polycondensation of silanes," *Journal of colloid and interface science*, vol. 540, pp. 554–562, 2019.

[21] A. Keller, K. Zainulabdeen, H. Warren, and M. in het Panhuis, "Fabrication of porous pdms sponges using spontaneously self-removing sacrificial templates," *MRS Advances*, vol. 7, no. 23-24, pp. 495–498, 2022.

[22] L. Peng, S. Yuan, G. Yan, P. Yu, and Y. Luo, "Hydrophobic sponge for spilled oil absorption," *Journal of applied polymer science*, vol. 131, no. 20, 2014.

[23] L. Gong, Y. Wang, X. Cheng, R. Zhang, and H. Zhang, "A novel effective medium theory for modelling the thermal conductivity of porous materials," *International Journal of Heat and Mass Transfer*, vol. 68, pp. 295–298, 2014.